

THERMAL-HYDRAULIC ANALYSIS OF FERROFLUID LAMINAR FLOW IN TUBE UNDER NON-UNIFORM MAGNETIC FIELD CREATED BY A PERIODIC CURRENT-CARRYING WIRE

Abderraouf Dahmani^{a,*}, José Muñoz-Cámara^b, Juan Pedro Solano^b, Samir Laouedj^a

^aLaboratory of Materials and Reactive Systems, University Djillali Liabes, Sidi Bel Abbes, 22000, Algeria.

^bDep. Ingeniería Térmica y de Fluidos, Universidad Politécnica de Cartagena Campus Muralla del Mar, Cartagena, 30202, Spain.

ABSTRACT

In this paper, a steady and laminar flow of ferrofluid ($Fe_3O_4/Water$) in a uniformly heated tube under the effect of non-uniform magnetic field arranged periodically along the tube is numerically analyzed using the finite volume method. The analysis sheds light on the flow pattern, Nusselt number, friction factor and the Performance Evaluation Criterion, at laminar flow regime ($10^2 \leq Re \leq 10^3$) and for various magnetic numbers ($Mn = 0, 2.83 \cdot 10^4, 6.37 \cdot 10^4$ and $1.13 \cdot 10^5$). The obtained results show that the magnetic field generated by periodic arrangement of the wire pitches, forces the flow to behave periodically as a result of the counter-rotating vortices and its periodic fluctuations due the Kelvin body force distribution. As a consequence, the Nusselt number increased by up to 8 % comparing to the cases without magnetic field. Also, a noticeable low increment for the friction factor is noticed (0.5 %).

Keywords: Ferrofluid, Magnetic field, Current-carrying wire, Ferrohydrodynamics, Laminar flow, CFD.

1. INTRODUCTION

Convective heat transfer has noteworthy importance in many industrial applications, e.g., power plants, chemical processes or cooling systems. Many studies have been carried out to enhance the convective heat transfer in order to downsize the equipment, but also to reduce the power consumption. Mainly, the used techniques are grouped into two major methods (Alam and Kim, 2018): passive and active techniques. Passive techniques do not employ any external power, e.g., adding fins (Benabderrahmane *et al.*, 2016), adding baffles (Boonloi and Jedsadaratanachai, 2021) or dispersing nano particles in the heat transfer fluid (Poplaski *et al.*, 2017). On the other hand, active methods employ an external source of energy, some examples are rotating tubes (Abotsi and Kizito, 2020) or pulsating flows (Muñoz-Cámara *et al.*, 2021).

The employment of the magnetic field in many engineering applications shows an upward trend, such as the magnetohydrodynamics (MHD) applications like in the nuclear reactors and the metallurgy sector (Khan *et al.*, 2020). Likewise, the ferrohydrodynamics (FHD) applications are now witnessing an increased interest, in this context, the ferrofluids are attracting the researchers as promising heat transfer fluids (HTF), due to the enhancement of the base fluid thermal properties (thermal conductivity) and the flow controllability by applying magnetic forces (Yamaguchi, 2008). This compound technique combines a passive method (adding nanoparticles to a base fluid) and active method (applying an external magnetic field). A typical ferrofluid is, for example, a base fluid (such as oil or water) with added nano-sized ferromagnetic particles like Fe_3O_4 or Fe_2O_3/NiO (Shahsavari *et al.*, 2016, Soltanipour *et al.*, 2020). Regarding the magnetic field, it can be applied by many different tech-

niques: magnets (Shi *et al.*, 2020), a uniform magnetic field generated by an electromagnet (Bezaatpour and Goharkhah, 2020), a magnetic dipole (Ramzan *et al.*, 2021), gradient magnetic field (Mousavi *et al.*, 2020) or non-uniform magnetic field created by a current carrying wire (Aminfar *et al.*, 2013).

Several studies have been carried out by different research groups to characterize the ferrofluid flow in ducts with a magnetic field generated by a current-carrying wire. Shakiba and Vahedi, 2016 tested numerically the effect of a non-uniform magnetic field (MF) generated by a straight current-carrying wire on the flow of ferrofluid in the inner tube of a double pipe heat exchanger. They reported that the force (Kelvin body force) produced by the interaction between the MF and the ferrofluid generated secondary flows that boosted the convective heat transfer in the heat exchanger. Another study by Larimi *et al.*, 2016 investigated numerically the influence of the MF generated via multiple wires parallels to each other and perpendicular to the ferrofluid flow in a ribbed channel for laminar flow conditions and various wire configurations. It was found that the presence of the MF increases the Nusselt number (especially for low Reynolds numbers), but also the pressure drop. The maximum increase was observed for the arrangement of all wires under the channel. Yousefi *et al.*, 2021 analysed numerically the effect of the location and the number of straight current-carrying wires on flow pattern and the thermal-hydraulic characteristics of ferrofluid laminar flow in a flattened tube. The study concluded that the secondary flows generated by the MF improved the heat transfer coefficient and increased the pressure drop. In addition, the position of the wires plays a major role in the number and

* Corresponding author. Email: da.abderraouf@gmail.com

the size of the vortices generated. Moreover, the configuration with two parallel wires placed at the top and bottom parts of the tube (flat sides of the tube) provided the highest heat transfer coefficient and pressure drop. Soltanipour *et al.*, 2020 introduced a curved current-carrying wire as new configuration, the MF generated by this wire was applied on a ferrofluid flow in a curved pipe for various circumferential angles. The authors stated that the position, as well as the MF intensity, has an important impact on the convective heat transfer enhancement. In addition, the optimal wire angle depends on the MF intensity.

Most of the cited works analyzed the effect of the non-uniform magnetic field produced by a straight current-carrying wire on ferrofluid flows in different ducts and agreed on the potential of this technique to enhance the convective heat transfer significantly. However, the studies about the effect of the MF generated by a wire arrangement different from the widely studied straight wire are almost non-existent.

The present study sheds light on the effect of the magnetic field generated by a novel current-carrying wire setup on the thermal-hydraulic characteristics of ferrofluid flow in a smooth tube under uniform heat flux conditions. The wire is arranged so it periodically modifies its position along the tube. The study is performed numerically using ANSYS® FLUENT, 2016, for several cases under laminar flow conditions, $10^2 \leq Re \leq 10^3$, and Magnetic numbers varying from $Mn = 0$ to $Mn = 1.13 \cdot 10^5$.

2. METHODOLOGY

2.1. Problem description

Fig.1 illustrates the three dimensional scheme of the studied tube, which is characterized by its diameter, $D=0.066$ m, and total length, $L=3$ m.

The ferrofluid $Fe_3O_4/water$ (with spherical particles with diameter $d_p=10$ nm and a volume fraction $\varphi = 4\%$) flows in the z direction, with a uniform temperature $T = T_{in}$ and uniform velocity $V = V_{avg}$ at the inlet. The tube outer wall is exposed to a uniform heat flux, q'' .

To generate the magnetic field, the tube is equipped with a current-carrying wire with a periodic configuration, characterized by the pitch length, l , and the angle, θ , (see Fig.1). The fluid flow is modified by the magnetic field generated by the electrical current flowing through the current-carrying wire, I . Only the MF generated by the wires parallel to the tube is taken into consideration, neglecting the connections between wire pitches.

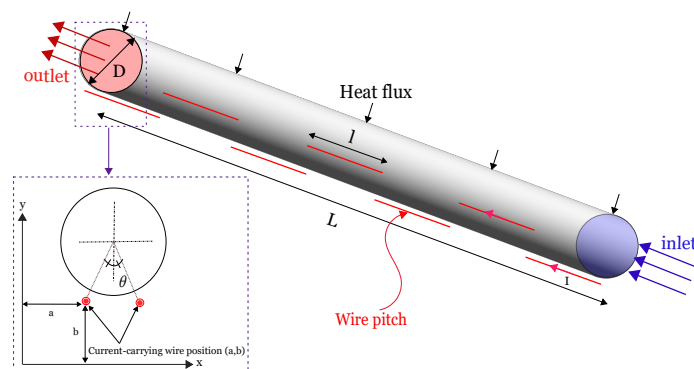


Fig. 1 3D model of the tube, the periodic current-carrying wire setup and pitch definition.

2.2. Governing equations

The single phase model is selected for this numerical investigation. The ferrofluid flow is considered to be laminar and steady, assuming that

Fe_3O_4 nanoparticles and water (base fluid) are in thermal equilibrium to each other and no slip velocity can be applied between them. Also, the ferrofluid is assumed to be homogeneous, Newtonian and incompressible.

In the presence of the MF, the electromagnetic force (Lorentz force) and magnetization force (Kelvin force) appear as resulting forces, representing the magnetohydrodynamics (MHD) and the ferrohydrodynamics (FHD) effects. Due to the negligible value of the electrical conductivity of the ferrofluid, the MHD terms are neglected from the governing equations in this study, as well as the magneto-caloric effect in the energy equation (Soltanipour *et al.*, 2020).

By considering the previous assumptions, the governing equations (continuity, momentum and energy equations) are simplified (Neuringer and Rosensweig, 1964, Shakiba and Vahedi, 2016, Sheikholeslami *et al.*, 2018):

$$\nabla \cdot (\rho_f \vec{V}) = 0 \quad (1)$$

$$\rho_f (\vec{V} \cdot \nabla \vec{V}) = -\nabla p + \mu_f \nabla^2 \vec{V} + \vec{F}_k \quad (2)$$

$$\vec{V} \nabla T = \frac{k_f}{\rho_f C_{p,f}} \Delta T \quad (3)$$

The term \vec{F}_k in the momentum equation (Eq. 2) represents the Kelvin force, where:

$$\vec{F}_k = \mu_0 (\vec{M} \cdot \nabla) \vec{H} \quad (4)$$

The following terms (Eq. (5) and (6)) represent the components of the force in the x and y directions, respectively:

$$F_k(x) = \mu_0 M \frac{\partial H}{\partial x} \quad (5)$$

$$F_k(y) = \mu_0 M \frac{\partial H}{\partial y} \quad (6)$$

H refers to the magnetic field intensity modulus and M represents the magnetization, which is given as (Mousavi *et al.*, 2020):

$$M = \frac{6\varphi m_p}{\pi d_p^3} \left(\coth(\xi) - \frac{1}{\xi} \right) \quad (7)$$

where m_p is the magnetic momentum (Eq. (8)) and ξ represents the Langevin parameter (Eq. (9)).

$$m_p = \frac{4\mu_B \pi d_p^3}{6 \times 91.25 \times 10^{-30}} \quad (8)$$

$$\xi = \frac{\mu_0 m_p H}{k_B T} \quad (9)$$

where Bohr's magneton $\mu_B=9.27 \times 10^{-24}$ A·m² and Boltzmann constant $K_B=1.3806503 \times 10^{-23}$ J/K.

2.3. Thermo-physical proprieties calculation

The thermo-physical properties of the ferrofluid are calculated using the thermo-physical properties of Fe_3O_4 nanoparticles and water (Table 1), via the following equations (Goharkhah and Ashjaee, 2014):

Table 1 The thermo-physical properties of the used materials (Malekan and Khosravi, 2018).

	Water (base fluid)	Fe_3O_4 (nanoparticles)
ρ (kg/m ³)	1024	5200
c_p (J/kg·K)	4001	670
k (W/m·K)	0.596	6
μ (kg/m·s)	0.00108	-

Ferrofluid density:

$$\rho_f = \varphi\rho_p + (1 - \varphi)\rho_b \quad (10)$$

Ferrofluid specific heat:

$$c_{p,f} = \varphi c_{p,p} + (1 - \varphi)c_{p,b} \quad (11)$$

Ferrofluid dynamic viscosity:

$$\mu_f = (1 + 2.5\varphi)\mu_b \quad (12)$$

Ferrofluid thermal conductivity:

$$k_f = \left[\frac{k_p + (n-1)k_b - (n-1)\varphi(k_b - k_p)}{k_p + (n-1)k_b - \varphi(k_b - k_p)} \right] k_b \quad (13)$$

Where the empirical shape factor of the nanoparticles is taken as $n=3$ (spherical particles) (Shakiba and Vahedi, 2016).

2.4. Numerical solution procedure and boundary conditions

To solve the governing equations, the finite volume method is adopted using a commercial Computational Fluid Dynamics code ANSYS® FLU-ENT, 2016. SIMPLEC algorithm is selected and the simulation is performed in parallel mode using high performance computing hardware. The Kelvin body force components are implemented in the momentum equations like source terms (Eqs. (5) and (6) for x and y directions, respectively) using a user defined function (UDF). To ensure the quality of the results and as convergence criterion, the residuals are maintained below 10^{-6} for the continuity and momentum equations and 10^{-9} for the energy equation.

Regarding the applied boundary conditions, a uniform temperature $T_{in} = 300$ K and velocity V_{avg} (where, $10^2 \leq Re \leq 10^3$) are set at the inlet, a uniform heat flux $q''=2000$ W/m² is applied on the tube wall, while the outlet pressure is maintained as zero.

2.5. Data reduction

The apparent Darcy's friction factor is calculated according to its definition:

$$f = \frac{2\Delta P}{\rho_f V^2} \left(\frac{D}{L} \right) \quad (14)$$

where ΔP is the static pressure difference between the tube inlet and outlet, and L is the total length of the tube.

The average Nusselt number is calculated using Eq. (15) taking into consideration the axial variation of the heat transfer coefficient in the studied control volume.

$$Nu = \frac{h_{avg} D}{k} \quad (15)$$

The peripherally average heat convection coefficient, for each axial position, is calculated by:

$$\bar{h}(x) = \frac{q''}{\bar{T}_w(x) - T_b(x)} \quad (16)$$

where $\bar{T}_w(x)$ is the peripheral average of wall temperature at x , the axial position:

$$\bar{T}_w(x) = \frac{\sum_{i=1}^{n_{nodes}} T_i(x)}{n_{nodes}}; \forall i: r_i = D/2 \quad (17)$$

and $T_b(x)$ refers for the bulk temperature defined in Çengel and Ghajar, 2015, at the axial position x :

$$T_b(x) = \frac{\sum_{i=1}^{n_{cells}} \rho_i c_{pi} T_i(x) u_i(x) A_i}{\dot{m} c_p} \quad (18)$$

The Reynolds number is calculated as:

$$Re = \frac{\rho V D}{\mu} \quad (19)$$

The Prandtl number:

$$Pr = \frac{\mu c_p}{k} \quad (20)$$

The Performance Evaluation Criterion (Aghamiri *et al.*, 2021) is computed as:

$$PEC = \frac{(Nu/Nu_s)}{(f/f_s)^{1/3}} \quad (21)$$

For this study, another dimensionless number should be introduced to quantify the effect of the MF strength on the flow behaviour. The definition for the Magnetic number proposed by Soltanipour *et al.*, 2020 is used:

$$Mn = \frac{\mu_0 \chi H_r^2 D^2}{\rho_f \nu_f^2} \quad (22)$$

where, χ is the magnetic susceptibility (for this study $\chi=0.34859$) and H_r is the characteristic magnetic field (the magnetic field calculated at the tube wall point), and d is the distance between the current-carrying wire and the tube wall:

$$H_r = \frac{I}{2\pi d} \quad (23)$$

Although the position variation of the wire, H_r is constant along the axial direction, because the distance d is kept constant.

2.6. Mesh and model validation

To ensure the mesh independency, three different meshes, coarse mesh (1080000 elements), fine mesh (1948800 elements) and a very fine mesh (4377600 elements), were selected to perform a sensitivity study where the dimensionless axial velocity was used for the comparison. The three meshes were tested for ferrofluid flow in absence of the magnetic field at $Re = 100$. As it can be noticed in Fig.2, the obtained results for the fine mesh (Mesh #2) and the very fine mesh (Mesh #3) are identical while there is a deviation of 0.1 % between them and the coarse mesh (Mesh #1). Accordingly, the fine mesh was selected for its accuracy and to save the calculation time. The selected mesh is shown in Fig.3.

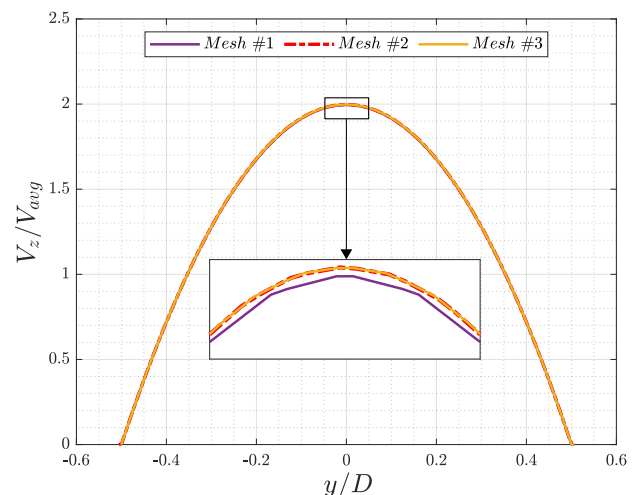


Fig. 2 Mesh independence study in term of dimensionless axial velocity for $Re = 100$ at the position $z/D = 30.3$.

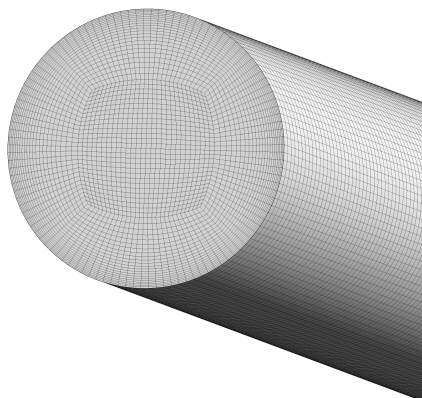


Fig. 3 Three dimensional view of the selected mesh.

In order to validate the numerical procedure and to check the accuracy of the results, the local Nusselt number for pure water is compared to the results obtained from known correlations (Churchill and Ozoe, 1973) for two different Reynolds numbers, $Re=100$ and $Re=1000$ in absence of the MF. The trends are plotted in Fig.4.

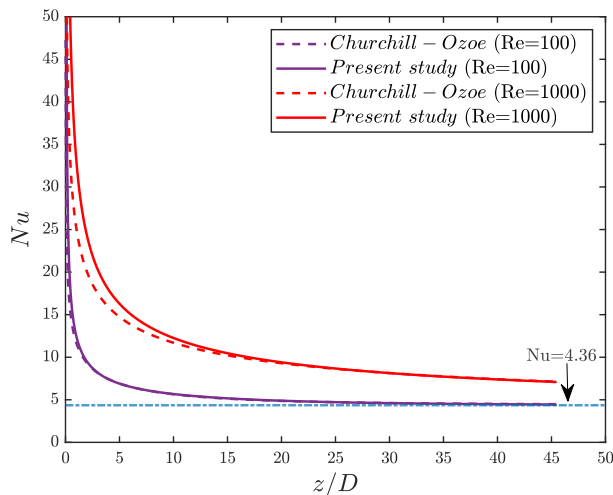


Fig. 4 The local Nusselt number for present study compared to the results of Churchill and Ozoe, 1973 correlation.

There is a good agreement between the results from the simulations and those calculated by the correlation, especially for the lower Reynolds number case. However, for the $Re=1000$ case a deviation lower than 18.6 %, is noticed at the region located between $z/D = 0$ and $z/D = 20$.

3. RESULTS AND DISCUSSION

3.1. Characteristics of the flow

To study the effect of the magnetic field on the ferrofluid flow, the axial velocity at the tube axis is measured along the tube length. The results for the case without magnetic field and for three different Magnetic numbers are shown in Fig.5.

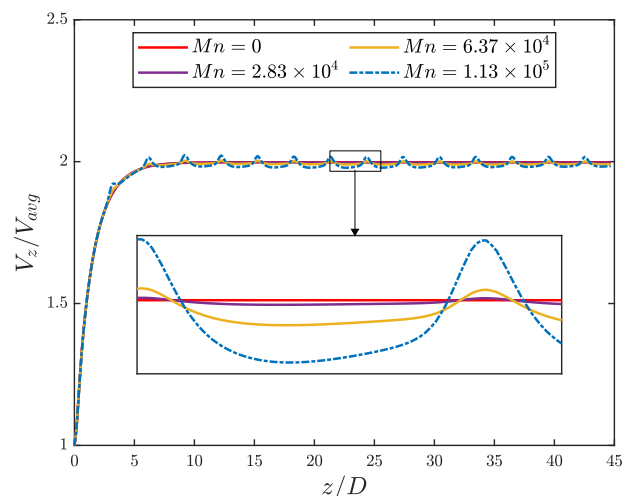


Fig. 5 Dimensionless axial velocity profile at tube center-line for different Magnetic numbers at $Re=100$.

For the case without magnetic field, there is an initial flow development from $V_z = V_{avg}$ (uniform velocity profile at the inlet) to $V_z = 2 \cdot V_{avg}$, corresponding to the theoretical solution for a fully-developed laminar flow (Hagen–Poiseuille law). The theoretical value of the developing length is around $5 \cdot D$ (for $Re = 100$), close to the value where the axial velocity reaches a steady value.

When an external magnetic field is imposed, the velocity follows a periodic behaviour over the general trend of the case without magnetic field. The spatial periodicity of the velocity matches the length of the wire pitch, $l = 3 \cdot D$.

A zoom for one of the pitches (Fig.5) shows that the central axial velocity approaches a lower steady value, but the change of the wire position leads to a sharp increase of the axial velocity. This pattern repeats for each wire pitch, because the wire position at each pitch is symmetric with respect to the tube center. The magnitude of the fluctuations is observed to be higher at higher Magnetic numbers.

For a better understanding of the velocity behaviour, the axial velocity contours for three different axial positions, $z/D = 37.1$, 41.1 and 43.2 are shown in Fig.6, which correspond to three different consecutive wire pitches. The axial contours do not show any changes for the case with no magnetic field because the flow is hydrodynamically developed. However, for the periodic wire with magnetic field, the fluid is attracted towards the wire, deforming the high velocity region towards the wire and, at the same time, decreasing the axial velocity at the tube center as was shown in Fig.5. When the wire changes its position, the flow has to redevelop again to be adapted to the new magnetic force applied to the fluid, reaching again a pattern which is symmetric to the previous pitch.

Fig.7 a-b show the three dimensional streamlines along the tube for $Re = 100$. As expected, in the absence of magnetic field the flow streamlines are straight (see Fig.7a). On the other hand, the application of the magnetic field ($Mn = 1.13 \cdot 10^5$) generates swirled flows (Fig.7b).

Furthermore, the visualized transversal streamlines in Fig.7c show the generation of secondary flows forming counter-rotating vortices due to Kelvin body forces. In addition, and as it can be noticed in the same figure, the vortices convergence point varies depending on the wire pitch position. However, these vortices intensify the transversal motion of the fluid from the tube wall toward the tube center.

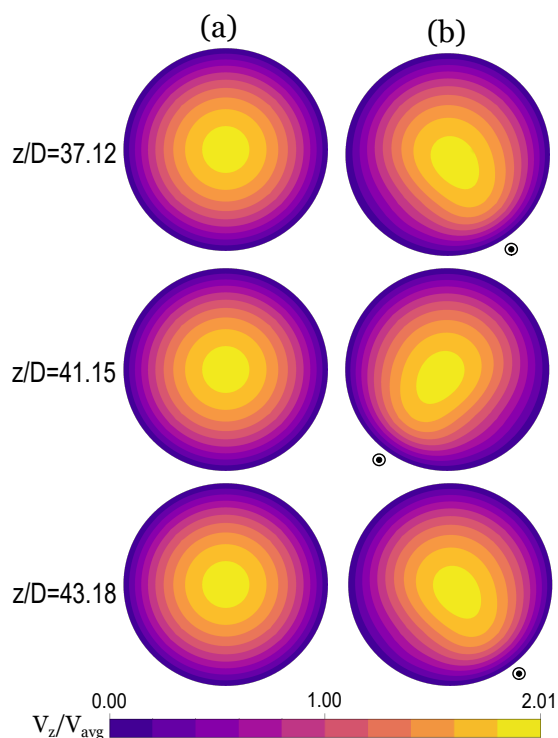


Fig. 6 Velocity contours at $Re=100$, (a) $Mn = 0$ (b) $Mn = 1.13 \cdot 10^5$.

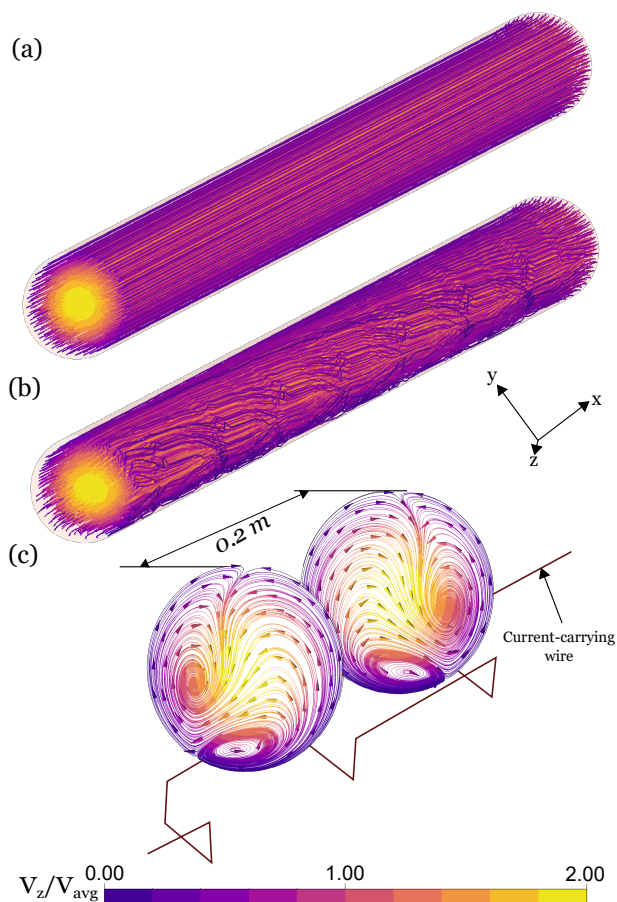


Fig. 7 The three dimensional streamlines, (a) $Mn = 0$, (b) $Mn = 1.13 \cdot 10^5$, (c) Transversal streamlines in presence of magnetic field $Mn = 1.13 \cdot 10^5$.

3.2. Thermo-hydraulic results

Three different Reynolds numbers covering the laminar region, $Re=100$, 500 and 1000 are simulated for four Magnetic numbers, ranging from 0 to $1.13 \cdot 10^5$. The Nusselt number and the increase in comparison to the case without magnetic field are included in Fig.8.

As can be seen, the magnetic field applied has a low influence for the two highest Reynolds numbers, while there is a significant enhancement, 8 %, for the lowest Reynolds number, $Re = 100$. This can be justified by the smallest weight of the magnetic forces when the inertial forces are increased (higher Reynolds number). This limits the potential interest of this application to relatively low Reynolds numbers, unless the electrical currents or the fraction of ferroparticles is significantly increased.

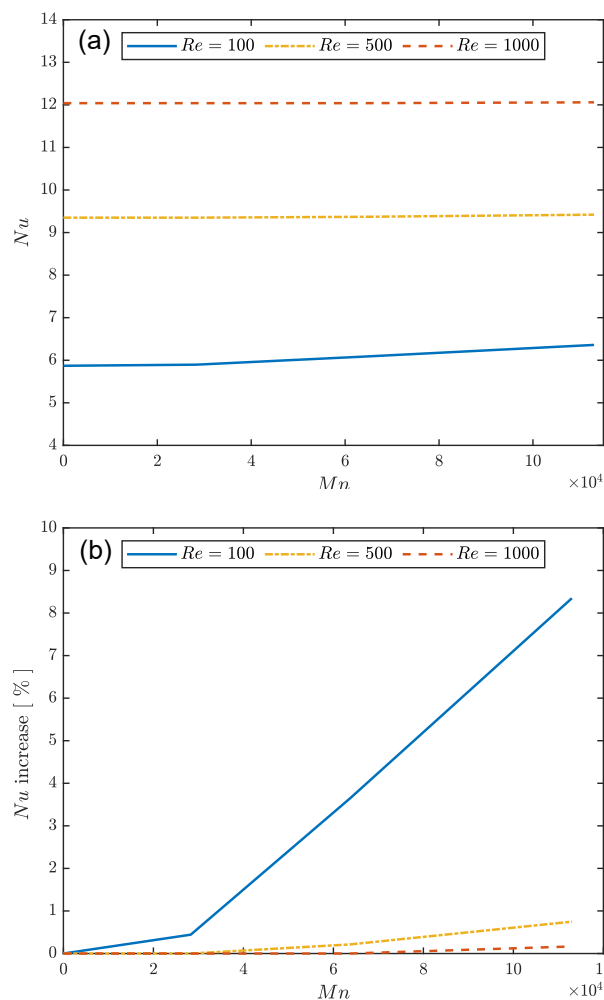


Fig. 8 Effect of magnetic field increment on the average Nusselt number for different Reynolds numbers.

To account for the effect of the magnetic forces on the pumping power, the average friction factor is calculated and plotted in Fig.9. As expected, there is a close relation between pressure drop and heat transfer, and every increase in the Nusselt number implies an increase in the friction factor. However, the friction factor augmentation is much lower than the Nusselt number increase, i.e., a slightly higher power consumption is necessary to increase significantly the heat transfer.

The widely used PEC (Performance Evaluation Criterion) is calculated to measure the heat transfer enhancement accounting for the increase in the friction factor (Fig.10). Due to the low increase in the friction factor for all the cases tested, the enhancement is quite similar to that

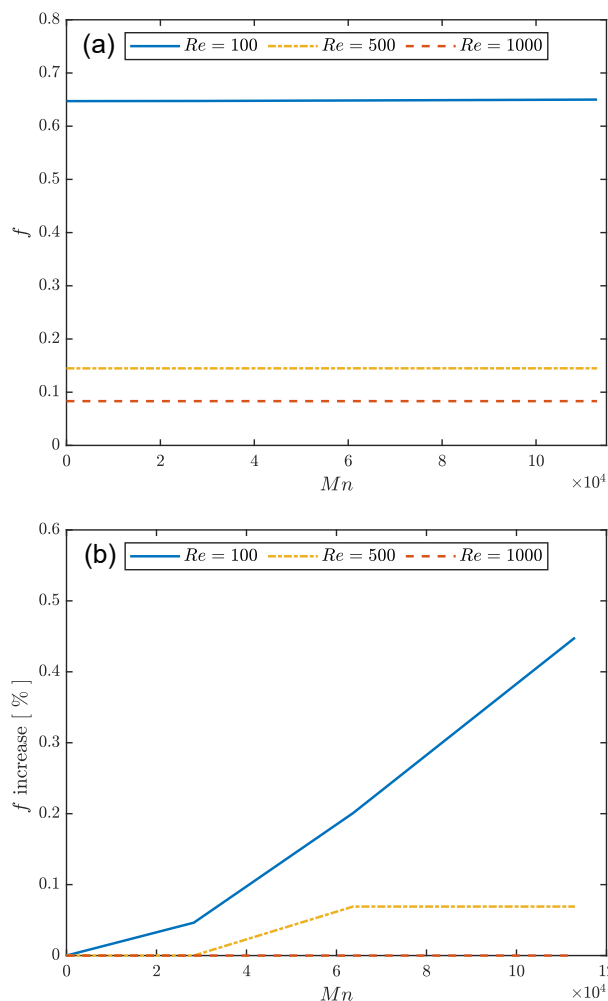


Fig. 9 Effect of magnetic field increment on the average friction factor for different Reynolds numbers..

obtained for the Nusselt number (Fig.8).

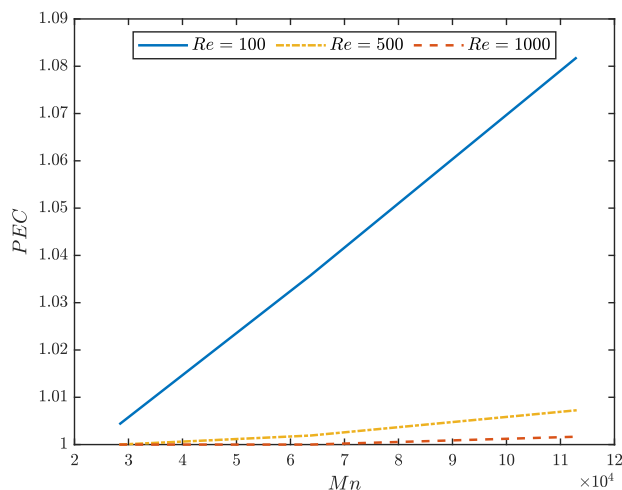


Fig. 10 Performance Evaluation Criterion (PEC) in function of the magnetic number (Mn).

The periodic wire introduces a significant enhancement, greater than a 5%, at the lowest Reynolds number tested, $Re = 100$, and for Magnetic numbers higher than $8 \cdot 10^4$.

It should be noticed that the tube length tested, $L = 45 \cdot D$, implies that the flow is thermally developing along all the tube for relatively low Reynolds numbers, $Re \approx 130$; while the periodic wire heat transfer enhancement is only noticeable in the developed region. Thus, a higher enhancement could be expected for longer tubes.

4. CONCLUSIONS

The main conclusions from this study are:

1. The magnetic field generated by the periodic wire has a negligible effect on the velocity behaviour along the hydrodynamically developing region, while it generates a noticeable periodic fluctuation on the flow pattern once the flow would have reached a steady solution.
2. The maximum increase observed in the Nusselt number is 8 % for $Re = 100$, in comparison to the same smooth tube without magnetic field.
3. There is a low increase in the friction factor, lower than 0.5 %, for all the tested cases.
4. The use of the periodic wire is recommended for tubes working on the laminar region with a significant portion of the tube length under fully-developed flow conditions, i.e., low Reynolds numbers or long tubes.

ACKNOWLEDGEMENTS

The first author gratefully acknowledges Universidad Politécnic de Cartagena for providing the high performance computing hardware, and Alberto Egea-Villarreal for his priceless help.

NOMENCLATURE

c_p	specific heat (J/kg K)
D	tube diameter (m)
D_e	absorber tube outer diameter (m)
d_p	particle diameter (m)
H	magnetic field intensity vector modulus (A/m)
H_r	characteristic magnetic field intensity (A/m)
h	heat transfer coefficient ($W/m^2 K$)
I	electric current (A)
k	thermal conductivity (W/m K)
K_B	Boltzmann constant (J/K)
L	tube length (m)
l	wire pitch length (m)
M	magnetization (A/m)
m_p	particle magnetic moment ($A m^2$)
P	pressure (Pa)
q''	heat flux (W/m^2)
T	temperature (K)
V_{avg}	mean axial velocity (m/s)
x, y, z	directions (m)
<i>Greek Symbols</i>	
α_f	thermal diffusivity (m^2/s)
φ	particle volume fraction
ξ	Langevin parameter
μ	dynamic viscosity (Pa s)
μ_0	vacuum permeability (T m/A)
μ_B	Bohr's magneton ($A m^2$)
ν	kinematic viscosity (m^2/s)
ρ	density (kg/m^3)

χ	magnetic susceptibility
<i>Superscripts</i>	
<i>b</i>	base fluid
<i>f</i>	ferrofluid
<i>in</i>	inlet
<i>p</i>	nanoparticle
<i>w</i>	wall

REFERENCES

- Abotsi, O.Y.W., and Kizito, J., 2020, "Turbulent heat transfer in an axially rotating pipe at high rotation rate: a numerical study," *Frontiers in Heat and Mass Transfer (FHMT)*, **14**.
<http://doi.org/10.5098/hmt.14.24>.
- Aghamiri, H., Niknejadi, M., and Toghraie, D., 2021, "Analysis of the forced convection of two - phase Ferro - nanofluid flow in a completely porous microchannel containing rotating cylinders," *Scientific Reports*, **11**, 1–18.
<https://doi.org/10.1038/s41598-021-97152-3>.
- Alam, T., and Kim, M.H., 2018, "A comprehensive review on single phase heat transfer enhancement techniques in heat exchanger applications," *Renewable and Sustainable Energy Reviews*, **81**, 813–839.
<http://doi.org/10.1016/j.rser.2017.08.060>.
- Aminfar, H., Mohammadpourfard, M., and Ahangar Zonouzi, S., 2013, "Numerical study of the ferrofluid flow and heat transfer through a rectangular duct in the presence of a non-uniform transverse magnetic field," *Journal of Magnetism and Magnetic Materials*, **327**, 31–42.
<https://doi.org/10.1016/j.jmmm.2012.09.011>.
- ANSYS® FLUENT, 2016, *Release 17.1, User's Guide*, ANSYS, Inc.
- Benabderrahmane, A., Aminallah, M., Laouedj, S., Benazza, A., and Solano, J.P., 2016, "Heat Transfer Enhancement in a Parabolic Trough Solar Receiver using Longitudinal Fins and Nanofluids," *Journal of Thermal Science*, **25**(5), 410–417.
<http://doi.org/10.1007/s11630-016-0878-3>.
- Bezaatpour, M., and Goharkhah, M., 2020, "Convective heat transfer enhancement in a double pipe mini heat exchanger by magnetic field induced swirling flow," *Applied Thermal Engineering*, **167**, 114801.
<https://doi.org/10.1016/j.applthermaleng.2019.114801>.
- Boonloi, A., and Jedsadaratanachai, W., 2021, "Thermal performance assessment in a circular tube fitted with various sizes of modified v-baffles: A numerical investigation," *Frontiers in Heat and Mass Transfer (FHMT)*, **16**.
<http://doi.org/10.5098/hmt.16.17>.
- Çengel, Y., and Ghajar, A., 2015, *Heat and Mass Transfer: Fundamentals & Applications*, McGraw Hill Education.
- Churchill, S.W., and Ozoe, H., 1973, "Correlations for Laminar Forced Convection with Uniform Heating in Flow over a Plate and in Developing and Fully Developed Flow in a Tube," *Journal of Heat Transfer*, **95**(1), 78–84.
<https://doi.org/10.1115/1.3450009>.
- Goharkhah, M., and Ashjaee, M., 2014, "Effect of an alternating nonuniform magnetic field on ferrofluid flow and heat transfer in a channel," *Journal of Magnetism and Magnetic Materials*, **362**, 80–89.
<https://doi.org/10.1016/j.jmmm.2014.03.025>.
- Khan, S.A., Hayat, T., and Alsaedi, A., 2020, "Entropy optimization in passive and active flow of liquid hydrogen based nanoliquid transport by a curved stretching sheet," *International Communications in Heat and Mass Transfer*, **119**, 104890.
<https://doi.org/10.1016/j.icheatmasstransfer.2020.104890>.
- Larimi, M.M., Ghanaat, A., Ramiar, A., and Ranjbar, A.A., 2016, "Forced convection heat transfer in a channel under the influence of various non-uniform transverse magnetic field arrangements," *International Journal of Mechanical Sciences*, **118**, 101–112.
<https://doi.org/10.1016/j.ijmecsci.2016.09.023>.
- Malekan, M., and Khosravi, A., 2018, "Investigation of convective heat transfer of ferrofluid using CFD simulation and adaptive neuro-fuzzy inference system optimized with particle swarm optimization algorithm," *Powder Technology*, **333**, 364–376.
<https://doi.org/10.1016/j.powtec.2018.04.044>.
- Mousavi, S.M., Biglarian, M., Darzi, A.A.R., Farhadi, M., Afrouzi, H.H., and Toghraie, D., 2020, "Heat transfer enhancement of ferrofluid flow within a wavy channel by applying a non-uniform magnetic field," *Journal of Thermal Analysis and Calorimetry*, **139**(5), 3331–3343.
<https://doi.org/10.1007/s10973-019-08650-6>.
- Muñoz-Cámara, J., Crespí-Llorens, D., Solano, J., and Vicente, P., 2021, "Baffled tubes with superimposed oscillatory flow: Experimental study of the fluid mixing and heat transfer at low net Reynolds numbers," *Experimental Thermal and Fluid Science*, **123**, 110324.
<https://doi.org/10.1016/j.expthermflusci.2020.110324>.
- Neuringer, J.L., and Rosensweig, R.E., 1964, "Ferrohydrodynamics," *The Physics of Fluids*, **7**(12), 1927–1937.
<https://doi.org/10.1063/1.1711103>.
- Poplaski, L.M., Benn, S.P., and Faghri, A., 2017, "Thermal performance of heat pipes using nanofluids," *International Journal of Heat and Mass Transfer*, **107**, 358–371.
<https://doi.org/10.1016/j.ijheatmasstransfer.2016.10.111>.
- Ramzan, M., Howari, F., Chung, J.D., and Kadry, S., 2021, "Irreversibility minimization analysis of ferromagnetic Oldroyd - B nanofluid flow under the influence of a magnetic dipole," *Scientific Reports*, **11**, 1–19.
<https://doi.org/10.1038/s41598-021-84254-1>.
- Shahsavari, A., Saghafian, M., Salimpour, M.R., and Shafii, M.B., 2016, "Experimental investigation on laminar forced convective heat transfer of ferrofluid loaded with carbon nanotubes under constant and alternating magnetic fields," *Experimental Thermal and Fluid Science*, **76**, 1–11.
<https://doi.org/10.1016/j.expthermflusci.2016.03.010>.
- Shakiba, A., and Vahedi, K., 2016, "Numerical analysis of magnetic field effects on hydro-thermal behavior of a magnetic nanofluid in a double pipe heat exchanger," *Journal of Magnetism and Magnetic Materials*, **402**, 131–142.
<https://doi.org/10.1016/j.jmmm.2015.11.039>.
- Sheikholeslami, M., Barzegar Gerdroodbary, M., Mousavi, S.V., Ganji, D.D., and Moradi, R., 2018, "Heat transfer enhancement of ferrofluid inside an 90° elbow channel by non-uniform magnetic field," *Journal of Magnetism and Magnetic Materials*, **460**, 302–311.
<https://doi.org/10.1016/j.jmmm.2018.03.070>.
- Shi, E., Ahangar Zonouzi, S., Aminfar, H., and Mohammadpourfard, M., 2020, "Enhancement of the performance of a NEPCM filled shell-and-multi tube thermal energy storage system using magnetic field: A numerical study," *Applied Thermal Engineering*, **178**, 115604.
<https://doi.org/10.1016/j.applthermaleng.2020.115604>.
- Soltanipour, H., Gharegöz, A., and Oskooee, M.B., 2020, "Numerical study of magnetic field effect on the ferrofluid forced convection and entropy generation in a curved pipe," *Journal of the Brazilian Society of*

Mechanical Sciences and Engineering, **42**(3), 1–15.
<https://doi.org/10.1007/s40430-020-2218-5>.

Yamaguchi, H., 2008, *Engineering Fluid Mechanics*, vol. 85 of *Fluid Mechanics and Its Applications*, SPRINGER.
<https://doi.org/10.1007/978-1-4020-6742-6>.

Yousefi, E., Nazif, H.R., Najafi Khaboshan, H., and Azarinia, A., 2021, “Non-Uniform Magnetic Field Effect on Forced Convection Heat Transfer of Flattened Tubes Using Two-Phase Mixture Model,” *Heat Transfer Engineering*, **42**(12), 1041–1058.
<https://doi.org/10.1080/01457632.2020.1766251>.